Thin Solid Films 776 (2023) 139862

Contents lists available at ScienceDirect

Thin Solid Films

journal homepage: www.elsevier.com/locate/tsf

Elastic constants of titanium carbide films using surface Brillouin scattering

C Sumanya [a,b,c,*], DM Wamwangi [b,c], K Jakata [b,c], JD Comins [b,c]

[a] Institute of Materials Science Processing and Engineering Technology, Chinhoyi University of Technology, P Bag, Chinhoyi 7724, Zimbabwe
[b] DST/NRF Centre of Excellence in Strong Materials, University of Witwatersrand, Johannesburg, WITS 2050, South Africa
[c] Materials Physics Research Institute, School of Physics, University of Witwatersrand, Johannesburg, WITS 2050, South Africa

ARTICLE INFO

Keywords:
Titanium carbide films
Elastic stiffnesses
Surface Brillouin scattering

ABSTRACT

Surface Brillouin scattering (SBS) from surface phonons has been used for determining the dispersion curves of guided acoustic modes propagating along titanium carbide (TiC) films. Dispersion curves have been obtained by varying both the layer thickness and the angle of incidence. Elastic stiffnesses for the TiC on silicon and TiC on silicon carbide systems were determined from a least-squares fitting procedure of the velocity dispersion curves and used to simulate the respective SBS spectra. For each system there is good agreement between measured and calculated SBS spectra.

1. Introduction

Performances of cutting tools can be increased by applying a coating to the tool. Titanium carbide (TiC) coatings are widely used in such applications owing to their excellent properties, such as high chemical stability (except in oxidizing acids), high thermal conductivity, high hardness and strength and good corrosion resistance. Typical applications of TiC coatings include cutting and milling tools, use on ball bearings to improve their hardness and lower the coefficient of friction [1] and for corrosion resistance on metallic structures. However, titanium-based alloys have poor oxidation resistance at high temperatures [2]. This limits the highest operating temperature for components made of titaniumi-based alloys to about 550 °C [3].

Research on the structure, morphology and chemical composition of TiC films is widely available in literature [4–7]. TiC crystallises in the sodium chloride type structure similar to titanium nitride [4,5]. The structure and mechanical properties of a TiC film can be influenced by deposition parameters such as substrate bias, radio frequency (RF) sputter power, deposition pressure and temperature [1,4,6,7] or by addition of gases such as oxygen [8].

Elastic properties provide useful information concerning fundamental interactions within the material, thus enabling interatomic potentials to be developed for computational modelling of materials with superior qualities. Elastic stiffnesses are related to the engineering moduli used to describe bulk mechanical properties. A study of these properties therefore leads to information that is of practical value to both the physicist and the engineer. Several techniques have been used thus far to measure elastic properties of materials, in particular, elastic stiffnesses. These include, amongst others, the ultrasonic method [9,10], the resonance method [11], the photo acoustic method [12], particle and x-ray scattering [13] and scanning acoustic microscopy [14]. In the present work the elastic properties of TiC films deposited on different substrates silicon (Si) and silicon carbide (SiC), are investigated using the surface Brillouin scattering (SBS) technique.

2. Theoretical aspects

SBS is a technique that relies upon the inelastic scattering of photons by thermally activated elastic waves in solids. It involves the study of surface acoustic waves and is important for the determination of elastic properties of opaque and near opaque materials. Acoustic waves can scatter light by two distinct mechanisms, the surface ripple and the elasto-optic mechanism. In the surface ripple mechanism the phonon vibrations cause the surface to appear as a moving grating, i.e. a ripple capable by itself of producing diffraction and changing the frequency of the incoming light by the Doppler effect without invoking any modulation of the dielectric constant in the interior of the crystal [15]. In the elasto-optic scattering mechanism the dynamic fluctuations in the strain field cause a fluctuating dielectric constant, resulting in inelastic scattering of light entering the solid. The optical transparency of the solid is the main determinant of the relative importance of these scattering mechanisms. The bulk elasto-optic scattering is larger than the

* Corresponding author at: Institute of Materials Science Processing and Engineering Technology, Chinhoyi University of Technology, P Bag, Chinhoyi 7724, Zimbabwe.
E-mail address: csumanya@cut.ac.zw (C. Sumanya).

https://doi.org/10.1016/j.tsf.2023.139862
Received 27 October 2022; Received in revised form 19 April 2023; Accepted 25 April 2023
Available online 28 April 2023

surface-ripple scattering mechanism for transparent media and for opaque materials the surface-ripple mechanism is dominant. In the case of thin opaque films the elastodynamic Green's function method, invoking the surface ripple mechanism for the inelastic scattering of light, is used to calculate the Brillouin spectrum for scattering from the surface acoustic excitations [16]. This method is applied to a film on a substrate system in order to extract the film's elastic constants by least squares fitting to the velocity dispersion curves of the system (ν vs. $q_{//}d$) where the surface wavevector $q_{\parallel} = (4\pi/\lambda_i)\sin\theta$, and the wave velocity $\nu = \omega/q_{\parallel}$.

For a thin opaque material, e.g., TiC, light scattering by surface ripple mechanism dominates that by elasto-optic coupling. At a given temperature T and frequency ω the SBS scattering efficiency $I(\omega)$ for the surface ripple mechanism is given by

$$I(\omega) = \frac{DT}{\omega}\mathrm{Im}\{\widetilde{G}_{33}(q_{\parallel},\omega)\}.$$

D is a factor that depends on the scattering geometry, incident photon frequency and the optical properties of the medium. $\widetilde{G}_{33}(q_{\parallel},\omega)$ is the component of the Fourier domain elastodynamic Green's function pertaining to force and response normal to the surface and is given by

$$\widetilde{G}_{33}(q_{\parallel},\omega) = \sum_{n=1}^{6}\frac{i}{\omega}\left(B^{-1}\right)_3^{(n)}U_3^n\exp\left(-iq_3^{(n)}d\right).$$

$U_3^{(n)}$ and $q_3^{(n)}$ are, respectively, the components of the mode polarization and the frequency dependant wave vector perpendicular to the film plane and d is the film thickness. $n = 1,\ldots,6$ refers to partial waves in the layer and $n = 7,8,9$ to outgoing partial waves in the substrate. A true surface wave (e.g. the Rayleigh wave (RSAW)) arises when the inverse of the boundary value matrix B^{-1} becomes singular and then a sharp line in the spectrum is visible [17]. The nature of the excitations depends on the real and complex values of the wavevectors $q_3^{(n)}$ $n = 7,8,9$ of the substrate partial waves. The solutions $n = 7,8,9$ have complex $q_3^{(n)}$ in the region before the edge of the Lamb shoulder, the transverse bulk wave threshold $\omega_T = q_{//}\nu_T$, while in the region after the longitudinal wave threshold $\omega_L = q_{//}\nu_L$, all substrate modes, transverse and longitudinal, are propagating bulk waves with real $q_3^{(n)}$. Between these limiting frequencies ω_T and ω_L, there are mixed modes with both complex and real values of $q_3^{(n)}$, $n = 7,8,9$. There may be sharp resonances where B^{-1} is small but non-zero, leading to a pseudo-surface acoustic wave and higher order resonances within the region of the Lamb shoulder. Variations of $U_3^{(n)}$ can have a modifying effect on the spectra.

A particular combination of over-layer and substrate determines the types of excitations, localised near the surface, which can be observed by the SBS technique. These SBS-observable excitations include amongst others, RSAWs, Sezawa waves (SWs) and pseudo Sezawa waves (pSWs). Thin supported films can be produced such that one has a slow on fast system where the transverse bulk wave velocity in the layer is smaller than that in the substrate. In most cases this corresponds to an elastically soft film on an elastically hard substrate but density plays an equally important role. Conversely one can have a fast on slow system. In the former case it is possible to extract the elastic constants from the SBS spectra since the range of acoustic excitations is much richer. The Rayleigh and one or more Sezawa waves usually provide sufficient information [18]. However in the case of a fast on slow system, the measurable excitations are few, making it difficult to extract the elastic constants. The velocity dispersion of the modes as a function of the product of surface wavevector and thickness ($q_{//}d$) has been simulated to demonstrate these effects [19].

Simulations of SBS spectra of TiC hard films on several substrates over a range of film thickness from 5 nm to 1000 nm, are presented by Sumanya et al. (2017) [20]. The two main categories of thin supported films, namely fast on slow and slow on fast, and their further classification into strongly and weakly stiffened or loaded systems are discussed. The experimental SBS results presented here are for titanium carbide on silicon (*TiC/Si*) and titanium carbide on silicon carbide (*TiC/SiC*) systems which have been classified as weak fast on slow and weak slow on fast systems, respectively. This is based on calculations in which the elastic properties of the TiC films are determined from Voigt-Reuss-Hill averaging procedures for polycrystalline films and employing the elastic stiffneses of single crystal TiC as discussed by Sumanya et al. (2017) [20]. These averages yield five distinct non-zero constants each, for polycrystalline aggregates with preferred orientation. For stiffnesses, the five distinct average constants are C_{11}, C_{12}, C_{13}, C_{33} and C_{44}. However the general elastic properties of polycrystalline aggregates with a random distribution of anisotropic crystallites of any symmetry classes are the same as those of the isotropic material [21,22].

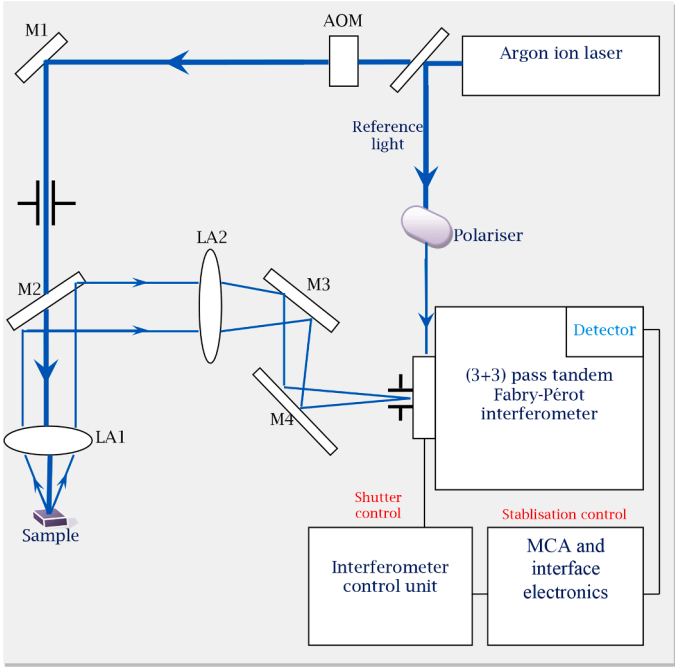

Fig. 1. Schematic diagram of the experimental arrangement used for surface Brillouin scattering spectroscopy. AOM and MCA stand for acoustic optic modulator and multi-channel analyser, respectively. M and LA represent mirrors and lenses, respectively.

3. Experimental aspects

3.1. Preparation and characterisation of the TiC films

TiC films, on both (100) single crystal Si and 6H (0001) SiC substrates with various thicknesses were synthesized using RF magnetron sputtering [23]. Films were prepared at 0.6 Pa with no substrate heating. Emphasis was given on optimising the quality of films for SBS studies. The films were characterized by X-ray reflectometry (XRR), glancing incidence X-ray diffraction (GIXRD) and X-ray photoelectron spectroscopy (XPS) to assess the quality of the films for SBS studies. Sputter rates were deduced for different powers. Density and roughness of the films were measured using XRR and stoichiometry of the films was verified by XPS measurements. The XRR, GIXRD and XPS measurements are discussed in detail elsewhere [23]. TiC films prepared by RF Magnetron sputtering have a random distribution of crystallites with no preferred orientation, as determined from GIXRD results [23]. As a result, only two nonindependent elastic stiffnesses (isotropic case [21,22]) can be used for the TiC films instead of five effective elastic stiffnesses

(polycrystalline aggregates with preferred orientation)

Table 1
Corresponding $q_{||}d$ values for film thicknesses d for *TiC/Si*.

d (nm)	50	100	200	300	400	500	600
$q_{||}d$	1.2	2.3	4.6	6.9	9.2	11.5	13.9

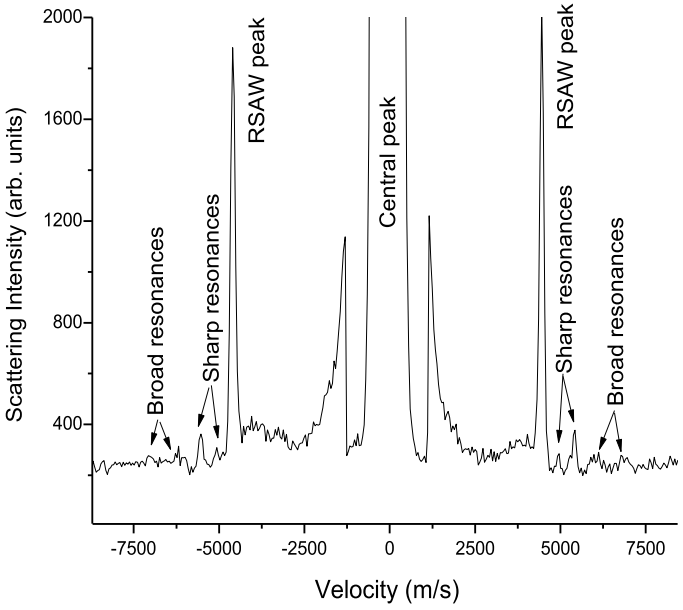

Fig. 2. Measured SBS spectrum for a 500 nm ($q_{||}d = 11.5$) TiC layer on a Si substrate. Both anti-Stokes and Stokes bands are shown. An intense RSAW is visible together with both sharp and broad features. The "Central peak" is the elastic peak resulting from elastically scattered light and is unshifted in frequency.

3.2. Usual set up for SBS measurements

For each experiment, the specimen was illuminated with the 514.5 nm line from an argon-ion laser and the spectrum of the scattered light was examined (Fig. 1). The incident laser light beam was of power 300 – 400 mW and was linearly polarised in the plane of incidence in all cases. In the backscattering arrangement used, a 120 mm focal length lens of aperture f/5.5 is used both for focusing the laser light onto the sample and for collecting the scattered light. The scattered light is analysed by the tandem interferometer and is then detected by a high efficiency silicon avalanche diode detector (EG&G Optoelectronics Canada SPCM-200-PQ) with a dark count of 1 per second.

3.3. Data capture and analysis

SBS spectra were acquired for TiC thin films in a backscattering configuration. The measurements were performed with the sample in air and at room temperature. Samples were mounted onto a goniometer, on which both the azimuthal angle (α) and the incident angle (θ) could be varied.

SBS measurements were carried out as a function of both θ (from 30° to 80° with the layer thickness constant at 500 nm) and layer thickness d (from 50 nm to 600 nm with the angle of incident constant at 71°). The tandem Fabry-Pérot interferometer (TFPI) was set up with a finesse of about 100 and a free spectral range (FSR) of 40 GHz. The spectral acquisition time for each sample was about 24 h on average. The acquisition time strongly depends on the optical alignment of the back-scattered light and the sample surface, so patience needed to be exercised with regard to the measurement period. The spectra were recorded by a Personal Computer-based multichannel analyser (MCA) interfaced with the TFPI and the detector. The MCA was supplied with software,

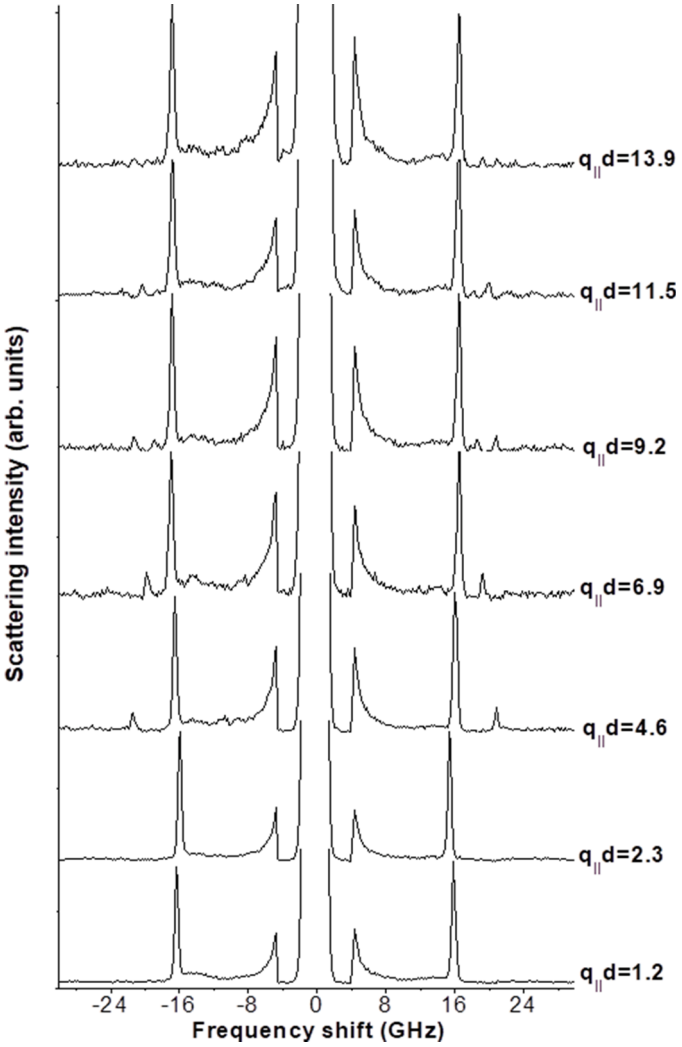

Fig. 3. Typical measured SBS results for scattering intensity as a function of frequency shift for TiC films on Si substrates.

GHOST *v.* 6.00 supplied by JRS Scientific Instruments. The software provides an easy way to acquire, save and analyse light spectrum data using an RS-232 communication system to pass the data to a common personal computer. The software includes functions for data analysis, spectrum calibration and curve-fitting. The other functions, data analysis and curve fitting were hardly used as spectra were always stored in ASCII format and later analysed using ORIGIN LAB *v.* 8 software.

4. Measured SBS spectra for TiC

4.1. Fast on slow system (TiC/Si)

A series of SBS measurements were carried out on the *TiC/Si* system for film thicknesses ranging from 50 nm to 600 nm. All the films were prepared at 200 W RF power. Table 1 shows the respective film thickness d of the deposited TiC films and the corresponding value of $q_{||}d$ obtained with incident angle θ_i kept constant at 71°. Fig. 2 shows a representative measured surface Brillouin spectrum for a film of thickness 500 nm in which $q_{||}d = 11.5$. Present in the spectrum is a relatively intense central peak and the associated Stokes and anti-Stokes bands. The RSAW of TiC is clearly identified together with two sharp and two broad features.

Fig. 3 shows typical measured results for the scattering intensity as a function of frequency shift, for the layer thickness given in Table 1 above. The spectra are identified by their respective $q_{||}d$ values (as in

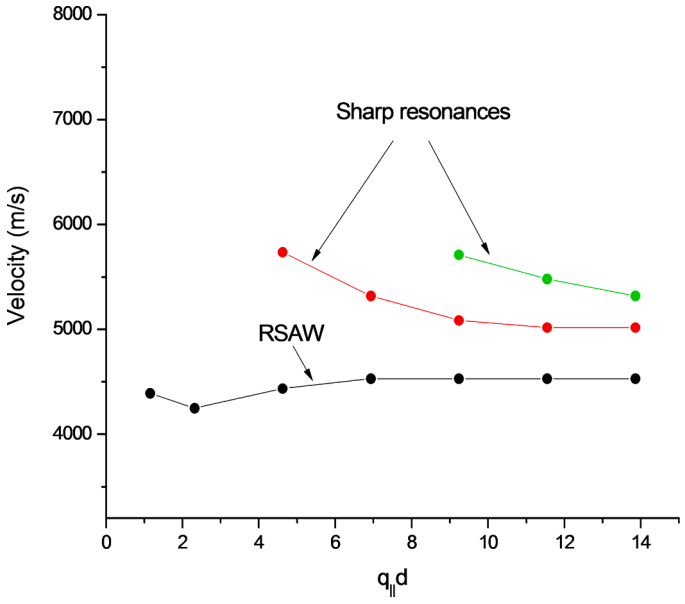

Fig. 4. Measured velocity dispersion of the modes vs. $q_{||}d$ for the *TiC/Si* system. The dispersion was obtained by varying the layer thickness d while keeping $q_{||}$ constant i.e., θ_i was kept constant at 71°.

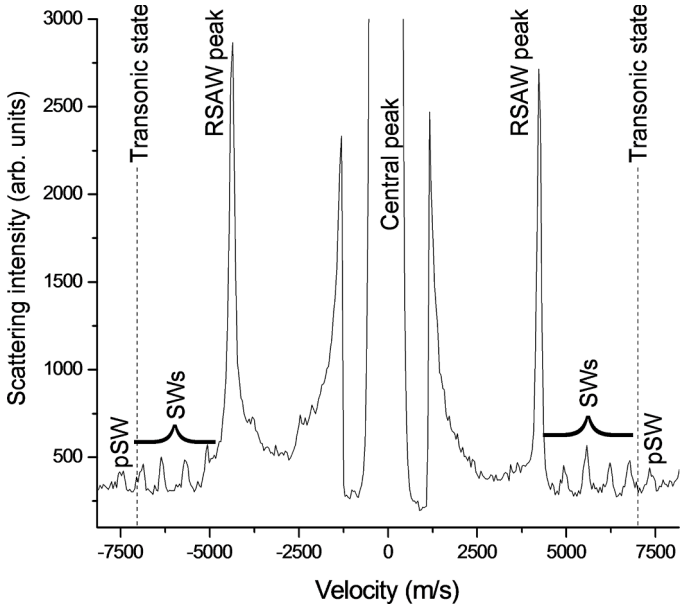

Fig. 5. Measured SBS spectrum for a 500 nm ($q_{||}d$ = 11.5) TiC layer on a SiC substrate. Anti-Stokes and Stokes bands are shown. An intense RSAW is visible together with SWs and a pSW. The "Central peak" is the elastically scattered peak.

Table 1). It is observed that, in addition to the RSAW which is dominant, other lower-intensity peaks appears at larger frequency shifts (> 16 GHz) for $q_{||}d \geq 4.6$.

A stiffening system is characterised by the film having a stiffening effect on the SAW velocity, i.e., with increasing layer thickness this velocity increases from the RSAW velocity of the substrate and levels off at the RSAW velocity of the film. This is visible in the measured dispersion curve for the *TiC/Si* system in Fig. 4. The dispersion was obtained by varying d whilst θ_i was kept constant at 71°.

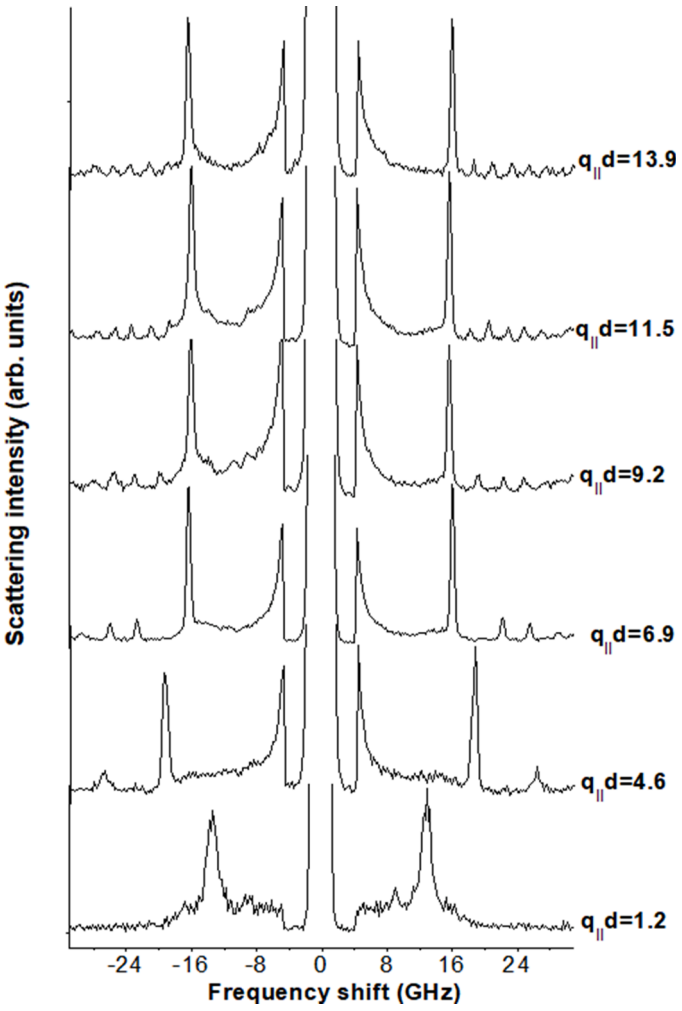

Fig. 6. Typical measured SBS results for scattering intensity as a function of frequency shift for TiC films on a SiC substrate. The broad feature at ~13 GHz is attributed to elasto-optic scattering.

4.2. Slow on fast system (TiC/SiC)

A series of SBS measurements were carried out on the *TiC/SiC* system for film thicknesses ranging from 50 nm to 600 nm. Fig. 5 shows a representative surface Brillouin spectrum as measured for a 500 nm TiC layer on a SiC substrate. The relatively intense central peak and associated Stokes and anti-Stokes bands are present, together with inelastic scattering peaks from the RSAW, SWs and a pSW which lies in the region above the transonic state [16].

The 6H-SiC (0001) substrate used in this work is transparent. In transparent solids, the elasto-optic scattering mechanism is dominant and therefore, if a transparent substrate is used elasto-optic scattering cannot be ignored [22,23]. The SBS results (Fig. 6) for $q_{||}d$ = 1.2 (layer thickness of 50 nm) show a broad feature around 13 GHz. This feature is assumed to be associated with the elasto-optic contribution from the substrate. The elasto-optic scattering mechanism is beyond the scope of this work and therefore only SBS measurements for films with $q_{||}d \geq 4.6$ (layer thickness of 200 nm and greater) were used in the extraction of elastic stiffnesses.

Table 2
Corresponding $q_{||}d$ values for film thicknesses d for *TiC/SiC*.

***d* (nm)**	50	200	300	400	500	600
$q_{||}d$	1.2	4.6	6.9	9.2	11.5	13.9

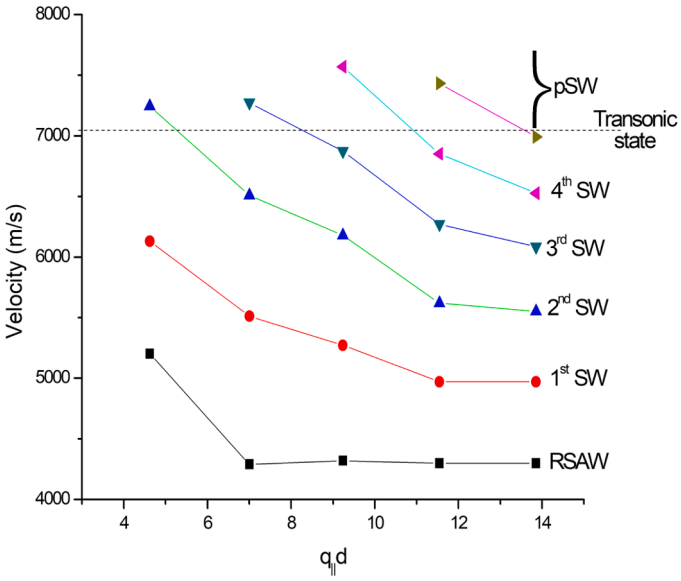

Fig. 7. Measured velocity dispersion of the modes vs. $q_{||}d$ for the *TiC/SiC* system. The dispersion was obtained by varying layer thickness *d*. $q_{||}$ was kept constant by keeping θ_i at 71°.

Fig. 6 shows typical measured results for scattering intensity as a function of frequency shift, for layer thicknesses in the range 50 nm to 600 nm. The spectra are identified by their respective $q_{||}d$ values as in Table 2

The dominant peak for each value of $q_{||}d$ (≥ 4.6) corresponds to the RSAW. As $q_{||}d$ is increased, the RSAW velocity first decreases and then levels off at 4320 m/s.

In this loading system the presence of the layer leads to a reduction of the RSAW velocity and to formation of film guided modes, SWs and pSWs. For $q_{||}d = 4.6$ only one SW is observed together with the Rayleigh, but as $q_{||}d$ increases more film guided modes are observed (up to five at $q_{||}d = 13.9$). The velocity dispersion of the modes as a function of $q_{||}d$ obtained from SBS measurements of five different layer thicknesses of TiC films is shown in Fig. 7.

5. Results

From SBS measurements, elastic stiffnesses of the film are extracted by the simultaneous fitting of the dispersion curves (surface wave velocity, *v*, as a function of $q_{||}d$) for the observed modes. The process of fitting the dispersion curves is one of inversion. The best fit is obtained by a least-squares minimization procedure, namely

$$\chi^2 = \sum_{SAWs} \left(v_i^{meas} - v_i^{calc}\right)^2$$

This minimisation is with respect to variations of the elastic stiffnesses in which v_i^{meas} are the measured SAW velocities and v_i^{calc} are the corresponding velocities determined from the surface Green's functions. Whenχ^2value is a minimum, the elastic stiffnesses used to calculate v_i^{calc} are taken as the elastic stiffnesses of the film.

The dispersion relations of the modes can be obtained either by varying *d* whilst $q_{||}$ is kept constant or vice versa. The dispersion curves discussed in Section 4 were obtained by varying *d*. A larger data set was obtained for both systems by including SBS measurements of a 600 nm layer as a function of θ_i (30° to 80°). The results obtained from both varying *d* whilst keeping $q_{||}$ constant and varying $q_{||}$ with *d* constant, are shown in Fig. 8.

Assuming an isotropic case, the Voigt-Reuss-Hill averaged elastic stiffnesses of TiC are $C_{11} = 492$ GPa, $C_{12} = 116$ GPa and $C_{44} = 188$ GPa. These have been calculated using single-crystal elastic stiffnesses of TiC:

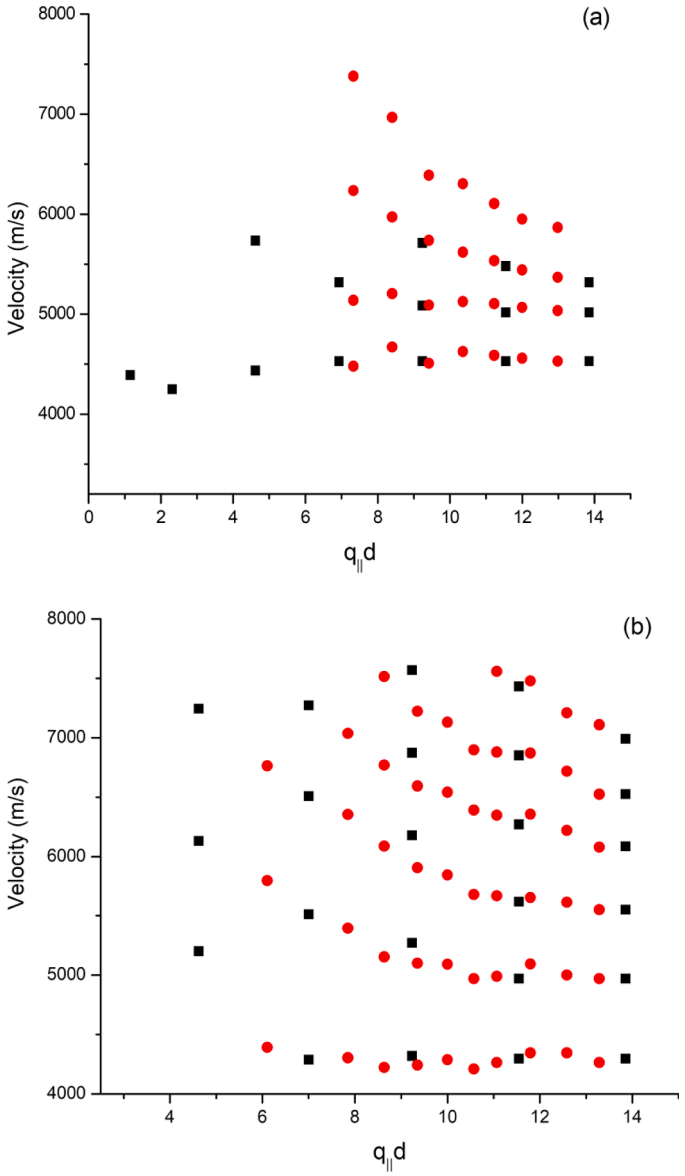

Fig. 8. Velocity dispersion curves for (a) *TiC/Si* and (b) *TiC/SiC*. Black squares are results obtained from variation of *d* whilst red circles correspond to the variation of $q_{||}$.

$C_{11} = 513$ GPa, $C_{12} = 106$ GPa and $C_{44} = 178$ GPa obtained from literature [22]. The averaged elastic stiffnesses were used as starting parameters in the minimization procedure on both systems. The resulting parameters are *TiC/Si*: $C_{11} = 270$ GPa, $C_{12} = 110$ GPa and $C_{44} = 83$ GPa and *TiC/SiC*: $C_{11} = 260$ GPa, $C_{12} = 104$ GPa and $C_{44} = 71$ GPa.

Brillouin scattering intensities were calculated using the elastic stiffnesses obtained and compared to the measured SBS results. The results are presented in Figs. 9 and 10 for *TiC/Si* and *TiC/SiC*, respectively. The density used in the fitting procedure for both systems is 3.4 g/cm^3; this was determined from X-ray reflectometry measurements [23]. Using the same elastic stiffnesses, SBS spectra were calculated (using Green's function methods) and compared to measured results as shown in Fig. 11. In each case only the anti-Stokes portion of the SBS spectrum is shown, with the intense central peak omitted for clarity. The figures show good agreement between measured and calculated velocities.

6. Discussion and conclusions

The elastic stiffnesses of TiC films determined from the two systems

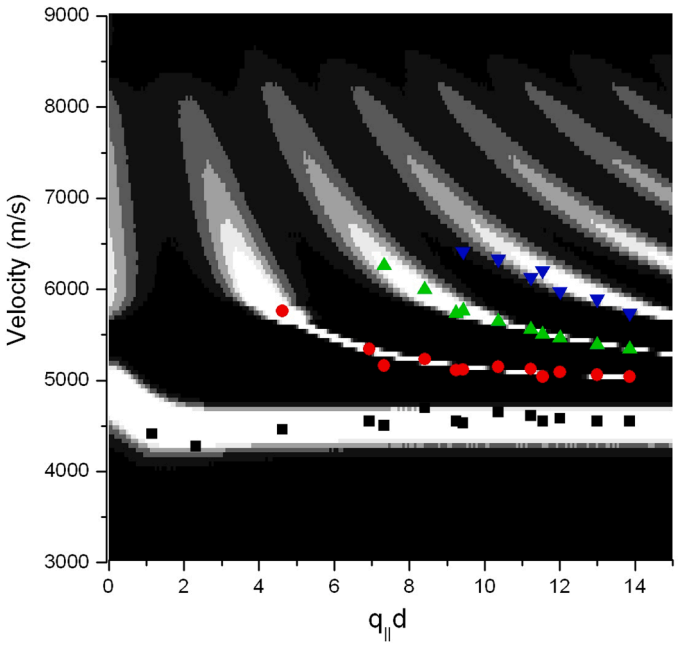

Fig. 9. Brillouin intensities compared to the measured results for the *TiC/Si* system. The elastic stiffnesses resulting from the best fit are C_{11} = 270 GPa, C_{12} = 110 GPa and C_{44} = 83 GPa.

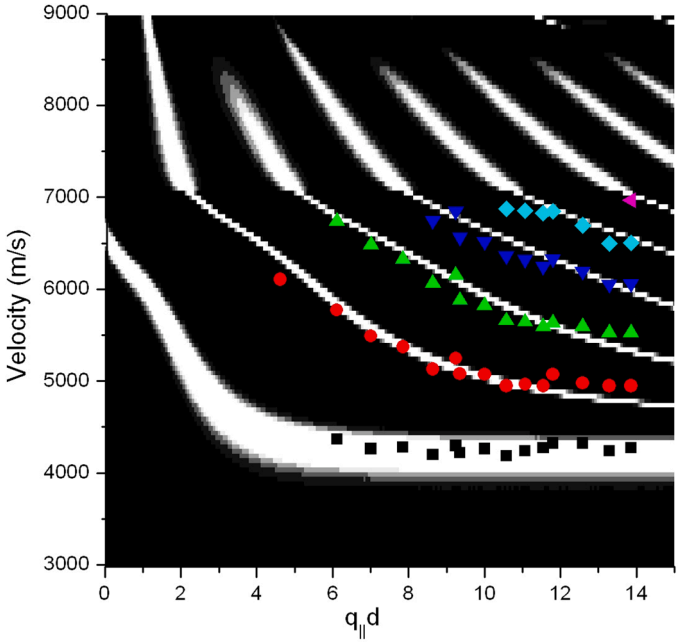

Fig. 10. Brillouin intensities compared to the measured results for the *TiC/SiC* system. The elastic stiffnesses resulting from the best fit are C_{11} = 260 GPa, C_{12} = 104 GPa and C_{44} = 71 GPa.

are presented in Table 3. These elastic stiffnesses have been determined using the least squares fitting to the phase velocities of the observed modes. This procedure has been used in many cases [24–28]. In most of these cases a slow on fast system was desirable due to a wide range of observable-acoustic excitations. In the present work elastic stiffnesses of TiC films have been determined using both slow on fast and fast on slow systems. The discrepancy in the elastic stiffnesses from the two systems can be explained in terms of the bonding between film and substrate. Nizzoli et al. [29], provided evidence that films may not be firmly

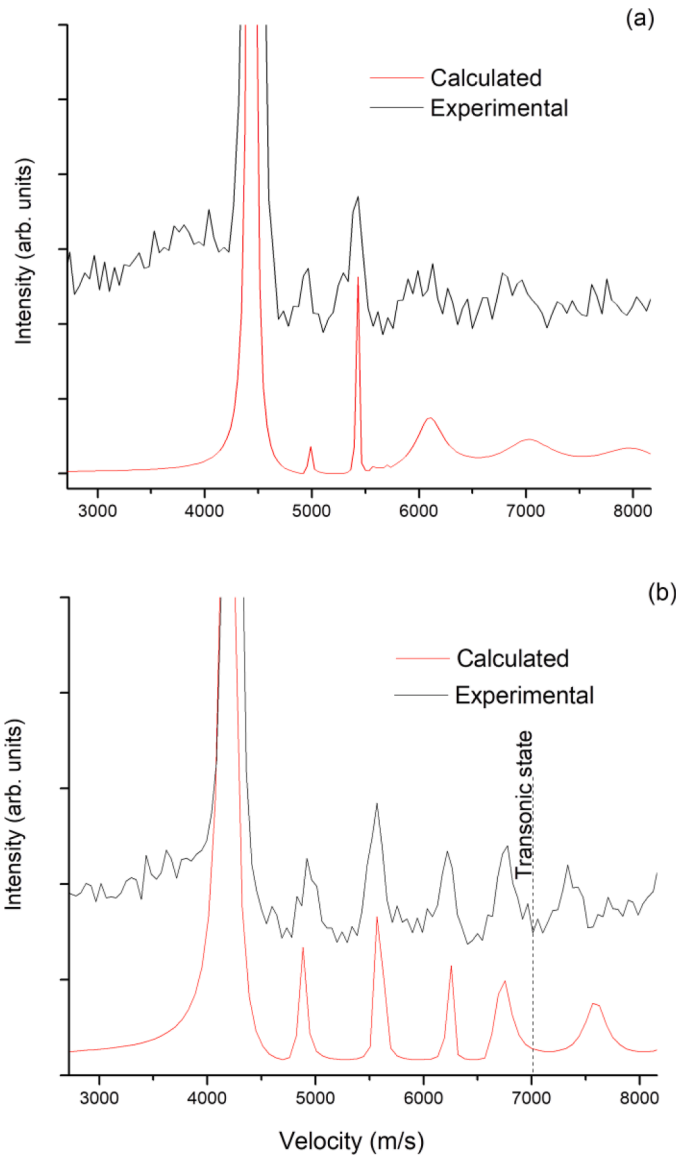

Fig. 11. Calculated and measured SBS spectra for a 500 nm TiC film on a (a) Si and (b) SiC substrate. The calculated spectra use the values of elastic stiffnesses obtained from fitting of the dispersion curves.

Table 3
Room temperature elastic stiffnesses of TiC films.

	C_{11} (GPa)	C_{44} (GPa)	C_{12} (GPa)
TiC/Si	270±3	83±2	110±3
TiC/SiC	260±3	71±2	104±3
Deviation	4%	14%	5%

bonded to the substrate in some cases. This can lead to serious errors in any type of fitting procedure. This was also confirmed by Yu et al. [30] who found that deposited thin films were neither perfectly bonded to nor in perfectly frictionless contact with the substrate. It was concluded that for a given minimum film thickness and a given substrate stiffness, the elastic stiffnesses of the film may be determined within a certain accuracy for the cases when the film is perfectly bonded to or in frictionless contact with the substrate. Although the bonding seems to be important, the degree of bonding may not always be easily detectable. The discrepancy in the elastic stiffnesses determined from two systems, *TiC/Si* and *TiC/SiC* is not unexpected. A relatively large discrepancy is

observed for C_{44} which is known to be sensitive to surface acoustic wave velocities [31].

CRediT authorship contribution statement

C Sumanya: Writing – original draft, Investigation, Visualization, Validation, Writing – review & editing, Data curation. **DM Wamwangi:** Software, Validation, Visualization. **K Jakata:** Visualization, Writing – review & editing. **JD Comins:** Supervision.

Declaration of Competing Interest

I CLEMENCE SUMANYA declare that there are no competing financial interests or personal relationships that could have appeared to influence the work reported in this paper.

Data availability

Data will be made available on request.

Acknowledgment

The authors thank the DST/NRF Centre of Excellence in Strong Materials (CoE-SM), South Africa for financial Support.

References

[1] J. Soldán, J. Musil, Structure and mechanical properties of DC magnetron sputtered TiC/Cu films, Vacuum 81 (2006) 531, https://doi.org/10.1016/j.vacuum.2006.07.013.
[2] X. Hou, X. Liu, M. Guo, K. Chou, A theoretical analysis for oxidation of titanium carbide, J. Mater. Sci. 43 (2008) 6193, https://doi.org/10.1007/s10853-008-2928-z.
[3] D. Vojtěch, B. Bártová, T. Kubatík, High temperature oxidation of titanium–silicon alloys, Mat. Sci. Eng. A361 (2003) 50, https://doi.org/10.1016/S0921-5093(03)00564-1.
[4] A. Mani, P. Aubert, F. Mercier, H. Khodja, C. Berthier, P. Houdy, Effects of residual stress on the mechanical and structural properties of TiC thin films grown by RF sputtering, Surf. Coat. Technol. 194 (2005) 190, https://doi.org/10.1016/J.SURFCOAT.2004.06.017.
[5] S. Kataria, S. Dash, A.K. Tyagi, Effect of adhesive and cohesive strength on the tribological behaviour of non-reactively sputtered TiC thin films, Surf. Interface Anal. 42 (2010) 7, https://doi.org/10.1002/SIA.3128.
[6] T. Obabta, K. Sato, M. Chiba, M. Mohri, T. Yamashina, K. Yabe, TiC coatings deposited onto carbon and molybdenum surfaces by electron beam evaporation, Thin Solid Films 87 (1982) 207, https://doi.org/10.1016/0040-6090(82)90358-3.
[7] C. Aguzzoli, C.A. Figueroa, G.V. Soares, I.J. Baumvol, Physicochemical and structural characteristics of TiC and VC thin films deposited by DC reactive magnetron sputtering, J. Mater. Sci. 45 (2010) 4994, https://doi.org/10.1007/S10853-010-4364-0.
[8] L.S. Marques, A.C. Fernandes, F. Vaz, M.M. Ramos, Influence of oxygen addition on the structural and elastic properties of TiC thin films, Plasma Process. Polym. 4 (2007) S195.
[9] H.F. Pollard, Sound Waves in Solids, Pion, London, 1977.
[10] E. Schreiber, O.L. Anderson, M. Soga, Elastic Constants and Their Measurement, McGraw-Hill, New York, 1973, https://doi.org/10.1115/1.3423687.
[11] O.L. Anderson, D. Isaak, H Oda, High-temperature elastic constant data on mnerals relevant to geophysics, Rev. Geophys. 30 (1992) 57, https://doi.org/10.1029/91RG02810.
[12] J.D. Aussel, J.P. Monchalin, Precision laser-ultrasonic velocity-measurement and elastic constant determination, Ultrasonics 27 (1989) 165, https://doi.org/10.1016/0041-624X(89)90059-0.
[13] K. Clausen, W. Hayes, M.T. Hutchings, J.K. KJems, J.E. Macdonald, R. Osborn, Lattice dynamics and elastic constants of uranium dioxide at high temperatures investigated by neutron scattering, High Temp. Sci. 19 (1985) 189. https://orca.cardiff.ac.uk/id/eprint/47847.
[14] M. Mendik, S. Satish, A. Kulik, G. Gremaud, P. Wachter, Surface acoustic wave studies on single-crystal nickel using Brillouin scattering and scanning acustic microscope, J. Appl. Phys. 71 (1992) 2830, https://doi.org/10.1063/1.351013.
[15] Sandercock J.R. and Nizzoli F. 1990 Surface brillouin scattering from phonons in dynamic properties of solids, edited by Horton G K and Maradudin AA. North-Holland, Amsterdam 281–335.
[16] X. Zhang, J.D. Comins, A.G. Every, P.R. Stoddart, W. Pang, T.E. Derry, Surface Brillouin scattering study of the surface excitations in amorphous silicon layers produced by ion bombardment, Phys. Rev. B 58 (1998) 13677, https://doi.org/10.1103/PhysRevB.58.13677.
[17] J.D. Comins, A.G. Every, P.R. Zhang, J.C. Crowhurst, G.R. Hearne, Surface Brillouin scattering studies of opaque solids and thin supported films, Ultrasonics 38 (2000) 450, https://doi.org/10.1016/S0041-624X(99)00199-7.
[18] P. Djemia, F. Ganot, P. Moch, V. Branger, P. Goudeau, Brillouin scattering investigation of elastic properties of Cu–Mo solid solutions thin films, J. Appl. Phys. 90 (2001) 756, https://doi.org/10.1063/1.1378331.
[19] C. Sumanya, J.D. Comins, A.G. Every, Surface Brillouin scattering in opaque thin films, J. Phys. Conf. Ser. 92 (2007), 012103, https://doi.org/10.1088/1742-6596/92/1/012103.
[20] C. Sumanya, J.D. Comins, A.G. Every, Surface Brillouin scattering in Titanium Carbide films, Wave Motion 68 (2017) 78, https://doi.org/10.1016/j.wavemoti.2016.08.011.
[21] A.G. Every, The elastic properties of solids: static and dynamic principles, in: M. Levy, H. Bass, R. Stern (Eds.), Handbook of Elastic Properties of Solids, Liquids and Gases (Vol. 1), Academic Press, New York, 2001.
[22] W. Pang, Measurement of Elastic Properties of Hard Films Using Brillouin Scattering, University of the Witwatersrand, Johannesburg, 1997. PhD Thesis.
[23] C. Sumanya, D.M. Wamwangi, J.D. Comins, Preparation and characterisation of titanium carbide thin films for surface brillouin scattering studies, J. Mater. Environ. Sci. 11 (5) (2020) 808. http://www.jmaterenvironsci.com/Document/vol11/vol11_N5/JMES-2020-1173-Sumanya.pdf.
[24] V. Bortolani, A.M. Marvin, F. Nizzoli, G. Santoro, Theory of Brillouin scattering from surface acoustic phonons in supported films, J. Phys. C. Solid State Phys. 16 (1983) 1757, https://doi.org/10.1088/0022-3719/16/9/018.
[25] A.M. Marvin, V. Bortolani, F. Nizzoli, Surface Brillouin scattering from acoustic phonons: I general theory, J. Phys. C Solid State. Phys. 13 (1980) 299, https://doi.org/10.1088/0022-3719/13/2/017.
[26] P. Mutti, Z. Sklar, G.A. Briggs, C Jeynes, Elastic properties of GaAs during amorphization by ion implantation, J. Appl. Phys. 77 (6) (1995) 2388, https://doi.org/10.1063/1.358763.
[27] M.G. Beghi, C.E. Bottani, P.M. Ossi, T.A. Lafford, B.K. Tanner, Combined surface Brillouin scattering from X-ray reflectivity characterisation of thin metallic films, J. Appl. Phys. 81 (1997) 627, https://doi.org/10.1063/1.364207.
[28] T. Wittkowski, G. Distler, K. Jung, B. Hillebrands, J.D. Comins, General methods for the determination of the stiffness tensor and mass density of thin films using Brillouin light scattering: study of tungsten carbide films, Phys. Rev. B 69 (2004), 205401, https://doi.org/10.1103/PhysRevB.69.205401.
[29] F. Nizzoli, B. Hillebrands, S. Lee, G.I. Stegeman, G. Duda, G. Wegner, W. Knoll, Determination of the whole set of elastic constants of a polymeric Langmuir-Blodgett film by Brillouin spectroscopy, Phys. Rev. B 40 (1989) 3323, https://doi.org/10.1103/physrevb.40.3323.
[30] H.Y. Yu, S.C. Sanday, B.B. Rath, The effect of substrate on the elastic properties of films determined by the indentation test-axisymmetric boussinesq problem, J. Mech. Phys. Solid. 38 (6) (1990) 745, https://doi.org/10.1016/0022-5096(90)90038-6.
[31] X. Zhang, P.R. Stoddart, J.D. Comins, A.G. Every, High-temperature elastic properties of a nickel-based superalloy studied by surface Brillouin scattering, J. Phys. Condens. Matter 13 (2001) 228, https://doi.org/10.1088/0953-8984/13/10/320.